Journal of the Optical Society of America B
OPTICAL PHYSICS

Effects of photon scattering torque in off-axis levitated torsional cavity optomechanics

M. Bhattacharya,[1,*] B. Rodenburg,[1] W. Wetzel,[1] B. Ek,[1] and A. K. Jha[2]

[1]School of Physics and Astronomy, Rochester Institute of Technology, Rochester, New York 14623, USA
[2]Department of Physics, Indian Institute of Technology, Kanpur 208016, India
*Corresponding author: mb6154@gmail.com

Received 23 January 2017; revised 28 April 2017; accepted 28 April 2017; posted 3 May 2017 (Doc. ID 285304); published 25 May 2017

We consider theoretically a dielectric nanoparticle levitated in an optical ring trap inside a cavity and probed by an angular lattice, with all electromagnetic fields carrying orbital angular momentum. Analyzing the torsional motion of the particle about the cavity axis, we find that photon scattering from the trap beam plays an important role in the optomechanical system. First we show that the presence of the torque introduces an instability. Subsequently, we demonstrate that for bound motion near a stable equilibrium, varying the optical torque strength allows for tuning the linear optomechanical coupling. Finally, we indicate that the relative strengths of the linear and quadratic couplings can be detected directly by homodyning the cavity output. Our studies should be of interest to researchers exploring quantum mechanics using torsional optomechanics. © 2017 Optical Society of America

OCIS codes: (080.4865) Optical vortices; (140.4780) Optical resonators; (260.6042) Singular optics.

https://doi.org/10.1364/JOSAB.34.000C44

1. INTRODUCTION

Levitated systems have lately emerged as exciting platforms for exploring optomechanical effects such as cooling [1], sensing [2,3], and matter–wave interferometry [4]. A unique advantage presented by such systems is their lack of mechanical clamping to any substrate or support. One consequence of this feature is excellent isolation from environmental, particularly thermal, disturbances. Studies of linear mechanical oscillations of optically levitated particles have been carried out both with [5] and without [6] cavities. Torsional optomechanics of levitated particles has also been theoretically proposed [7,8] and experimentally realized [9].

In this paper we consider the torsional optomechanics of a levitated subwavelength-size dielectric nanoparticle confined in a ring trap in a cavity and probed by an azimuthal lattice, as shown in Fig. 1. This configuration was recently proposed as a rotational analog of linear cavity optomechanics, in the case where the particle is free to rotate fully about the cavity axis [10].

In contrast to previous work on torsional optomechanics [7–9], the oscillations in the proposed configuration are off-beam axis. All the optical beams in the configuration carry orbital angular momentum (OAM). As has been shown earlier, the photons scattered from such beams exert an optical torque on particles in vacuum [11]. In the present work we show that depending on the angular location of the particle, this torque can lead to an instability or enable tunable linear optomechanical coupling in the system. To support our analysis, we first present a quantum master equation for the physical configuration of interest. We then consider the ensuing Langevin equations in the classical limit, which provide quantitative details regarding stability and optomechanical coupling. To conclude, we demonstrate that homodyning the output of the cavity allows one to measure the amount of linear optomechanical coupling present in the system.

2. MODEL OF THE PHYSICAL CONFIGURATION

The configuration of interest is shown in Fig. 1. In this section we develop the mathematical model corresponding to the physical system, culminating in the presentation of the quantum master equation and the ensuing classical Langevin equations.

A. Electric Fields

The net electric field has four contributions:

$$\boldsymbol{E} = \boldsymbol{E}_t + \boldsymbol{E}_p + \boldsymbol{E}_c + \boldsymbol{E}_b, \tag{1}$$

where E_t is the electric field of the trap beam, E_p is the azimuthal lattice probe used to excite the cavity mode E_c, and E_b is the field of all the background modes into which photons scatter from the nanoparticle. We now describe each of these fields individually.

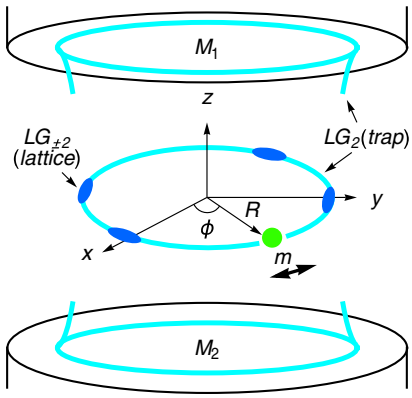

Fig. 1. Torsional optomechanical setup considered in this paper. A dielectric nanosphere of mass m is trapped on an optical ring of radius R created by a beam carrying OAM $l_t = 2$ and by an azimuthal lattice arising from the interference of two degenerate OAM $l = \pm 2$ beams. The resulting motion of the particle consists of harmonic oscillations about the beam axis. Mirrors M_1 and M_2 constitute the cavity.

1. Trap Field

The trap field is a Laguerre–Gaussian (LG) beam carrying OAM l_t,

$$\boldsymbol{E}_t = \boldsymbol{E}_0 \left(\frac{\rho}{R}\right)^{|l_t|} e^{\left(\frac{R^2-\rho^2}{2\omega_0^2} + il_t\phi - i\omega_t t\right)} \cos\left(\frac{\omega_t z}{c}\right) + \text{c.c.}, \tag{2}$$

where E_0 is the field amplitude, ρ is the cylindrical radial coordinate, $R = \omega_0\sqrt{l_t}$ is the radius at which the field intensity is a maximum at $z = 0$, ω_0 is the trap beam waist, ϕ is the cylindrical angular coordinate, ω_t is the trap beam frequency, and c is the speed of light. Here we have ignored the curvature of the beam wavefront as well as the contribution due to the Gouy phase.

2. Probe and Cavity Fields

The angular lattice in Fig. 1 arises from a superposition of two copropagating LG beams with OAM $\pm l$, beam waist ω_0, and degenerate frequencies $\omega_c \neq \omega_t$. The polarizations of the trap and probe beams will be assumed to be orthogonal, although we will not assign them explicit polarizations below. For the moment we consider the probe beam quantum mechanically,

$$\boldsymbol{E}_c = \sqrt{\frac{\hbar\omega_c}{\epsilon_0}}\psi(\boldsymbol{r})a + \text{h.c.}, \tag{3}$$

where a and $a^\dagger$ are the canonical creation and annihilation operators, respectively, of the cavity mode obeying the commutation rule $[a, a^\dagger] = 1$, with the mode function

$$\psi(\boldsymbol{r}) = \frac{1}{\sqrt{L_c\pi^2\omega_0^2|l|!}} \left(\frac{\rho}{\omega_0\sqrt{l}}\right)^{|l|} e^{\left(-\frac{\rho^2}{2\omega_0^2}\right)} \cos(l\phi)\cos\left(\frac{\omega_c z}{c}\right), \tag{4}$$

where L_c is the length of the cavity. The free-field Hamiltonian of this mode is

$$H_c^f = \hbar\omega_c a^\dagger a, \tag{5}$$

where we have dropped a factor of $1/2$ which has no dynamical significance. The probe is a field defined outside of the cavity and assumed to be mode-matched to the cavity mode at one of the mirrors. The energy of this mode is

$$H_p^f = \int_0^\infty \hbar\omega_p a_p^\dagger(\omega)a_p(\omega)\mathrm{d}\omega, \tag{6}$$

and its coupling with the cavity field is given by

$$H_{cp}^i = i\hbar\int_0^\infty \gamma(\omega)[a^\dagger a_p(\omega) - \text{h.c.}]\mathrm{d}\omega, \tag{7}$$

where $\gamma(\omega) \cong \sqrt{\kappa/\pi}$ is the coupling constant in terms of the cavity decay rate κ [12].

3. Background Fields

The background field is the continuum of modes that the nanoparticle scatters light into. In the plane wave basis the electric field is given by [13]

$$\boldsymbol{E}_b = i\sum_\mu \int \mathrm{d}^3\boldsymbol{k}\left(\frac{\hbar\omega_k}{16\pi^3\epsilon_0}\right)^{\frac{1}{2}} \boldsymbol{e}_\mu(\boldsymbol{k})a_\mu(\boldsymbol{k})e^{i\boldsymbol{k}.\boldsymbol{r}} + \text{h.c.}, \tag{8}$$

and the free field energy follows as

$$H_f^b = \sum_\mu \int \hbar\omega_k a_\mu^\dagger(\boldsymbol{k})a_\mu(\boldsymbol{k})\mathrm{d}^3\boldsymbol{k}, \tag{9}$$

where the index μ indicates the polarization of the photon.

4. Total Field Hamiltonian

The total field Hamiltonian is

$$H_{\text{field}}^f = H_c^f + H_p^f + H_{cp}^i + H_f^b. \tag{10}$$

B. Mechanical Degrees of Freedom

The Hamiltonian of mechanical motion is

$$\boldsymbol{H}_m^f = \frac{|\boldsymbol{p}|^2}{2\boldsymbol{m}} = \frac{\boldsymbol{p}_\rho^2}{2\boldsymbol{m}} + \frac{\boldsymbol{p}_z^2}{2\boldsymbol{m}} + \frac{\boldsymbol{L}_z^2}{2\boldsymbol{I}}, \tag{11}$$

where m is the mass; p_ρ and p_z are the radial and axial linear momenta, respectively; and L_z and $I = m\rho^2 \approx mR^2$ are the angular momentum and moment of inertia about the cavity (i.e., z) axis of the nanoparticle, respectively.

C. Optomechanical Interaction

The dielectric nanoparticle interacts with the total electric field through the induced dipole interaction given by

$$H_{\text{inf}}^i = -\frac{1}{2}\int_V \boldsymbol{P}(\boldsymbol{r})\cdot\boldsymbol{E}(\boldsymbol{r})\mathrm{d}^3\boldsymbol{r} \cong -\frac{\epsilon_0\epsilon_r}{2}V|\boldsymbol{E}|^2, \tag{12}$$

where $V = 4\pi r^3/3$ is the volume, r is the radius, and ϵ_r is the relative dielectric permittivity of the nanoparticle. A number of terms arise when Eq. (1) is used in Eq. (12). We will describe below the terms containing $|\boldsymbol{E}_t|^2$, $|\boldsymbol{E}_c|^2$, and $\boldsymbol{E}_t\cdot\boldsymbol{E}_b$ only, which yield the optical trap, the optomechanical coupling, and the scattering of photons from the trap beam, respectively. The remaining terms either vanish identically (due to the polarization orthogonality of the trap and probe beams) or are small shifts in position and frequency which we have absorbed into the appropriate definitions.

For the parameters considered in this paper, photon scattering from the probe is negligible in comparison to the scattering from the trap.

1. Optical Trap

Using Eq. (2) in Eq. (12), expanding around the points $q_\rho = \rho - R = 0$ and $q_z = z = 0$, up to second order in the coordinates, the optical trapping potential is given by

$$-\frac{\varepsilon_0 \boldsymbol{\varepsilon_r}}{2} V|\boldsymbol{E}_t|^2 = \frac{m}{2}(\omega_\rho^2 q_\rho^2 + \omega_z^2 q_z^2), \tag{13}$$

with radial and axial trapping frequencies

$$\omega_\rho = \sqrt{\frac{3\varepsilon_0 \varepsilon_r E_0^2}{\rho_m \omega_0^2}} \tag{14}$$

and

$$\omega_z = \sqrt{\frac{\varepsilon_0 \varepsilon_r E_0^2 \omega_t^2}{\rho_m c^2}}, \tag{15}$$

respectively, where ρ_m is the density of the nanoparticle. In this work, we will thus consider the particle trapped harmonically along the radial and axial directions and henceforth focus on the angular motion.

2. Optomechanical Coupling

The optomechanical coupling is found by expanding the corresponding term in Eq. (12) to the second order in the particle coordinates

$$-\frac{\varepsilon_0 \boldsymbol{\varepsilon_r}}{2} V|\mathbf{E}_c|^2 = \hbar g_l a^\dagger a (U_l + U_l^\dagger), \tag{16}$$

where the optomechanical coupling is

$$g_l = -\frac{2\omega_c \varepsilon_r V}{L_c \pi^2 \omega_0^2 |l|!} e^{-\frac{R^2}{\omega_0^2}}, \tag{17}$$

and an explicitly periodic angular displacement variable

$$U_l = e^{i2l\phi} \tag{18}$$

has been used. It can be shown readily that [14]

$$U_l|m\rangle = |m + 2l\rangle, \qquad U_l^\dagger|m\rangle = |m - 2l\rangle, \tag{19}$$

for angular momentum eigenstates $L_z|m\rangle = m\hbar|m\rangle$.

Combining the nanomechanical motion [Eq. (11)] with the optomechanical coupling [Eq. (16)] yields the Hamiltonian,

$$H_{OM} = \frac{\boldsymbol{L_z^2}}{2\boldsymbol{I}} \hbar g_l a^\dagger a (U_l + U_l^\dagger). \tag{20}$$

We note that the second term on the right-hand side of Eq. (20) yields a coupling nonlinear in the mechanical coordinate, since $U_l + U_l^\dagger = 2\cos 2l\phi$. As will be shown below, for small angular displacements and zero torque, this term yields a coupling quadratic in ϕ, which is then responsible for harmonic confinement of the nanoparticle. The ensuing frequency of mechanical oscillation then dynamically depends on the probe photon number $a^\dagger a$. Also, it will be shown that in the presence of the torque τ a coupling linear in ϕ can be generated.

D. Optical Scattering from the Trap

1. Scattering Hamiltonian

The Hamiltonian that describes the scattering of trap photons by the nanoparticle is given by

$$H_{\text{inf}}^i = -\frac{\varepsilon_0 \varepsilon_r}{2} \int_V \boldsymbol{E}_t(\boldsymbol{r}) \cdot \boldsymbol{E}_b(\boldsymbol{r}) \mathrm{d}^3\boldsymbol{r} \cong -\frac{\varepsilon_0 \varepsilon_r}{2} V \boldsymbol{E}_t(\boldsymbol{r}) \cdot \boldsymbol{E}_b(\boldsymbol{r}). \tag{21}$$

2. Dissipative Lindblad Operator

A long but straightforward calculation assuming a weak coupling to the background modes, fast decay of correlations in the bath presented by such modes, and employing the Born–Markov approximation yields using Eq. (21) the scattering contribution to the master equation [15],

$$\mathcal{L}_{\text{sc}}[\rho] = -\frac{\gamma_{\text{sc}}}{2} \sum_m \mathcal{D}[L_m]\rho, \tag{22}$$

where $\mathcal{L}_{\text{sc}}$ is the scattering Liouvillian, ρ is the system density matrix,

$$\mathcal{D}[L]\rho = \{L^\dagger L, \rho\} - 2L\rho L^\dagger \tag{23}$$

is the dissipation superoperator,

$$\gamma_{\text{sc}} = (\varepsilon_r V)^2 \frac{7\omega_t^3}{24\pi\hbar c^4} \left(\frac{c\varepsilon_0 E_0^2}{2}\right) \tag{24}$$

is the rate of trap photon scattering, and

$$L_m = \alpha_m U_m U_l \tag{25}$$

are the Lindblad operators, where

$$\alpha_{\text{m}} = \frac{6}{7} \int_0^1 \left(1 + \frac{x^2}{2}\right) J_m^2 \left(\frac{\omega_t R x}{c}\right) \mathrm{d}x, \tag{26}$$

and J_m is a Bessel function. For realistic parameters we find that $\gamma_{\text{sc}} \ll \gamma$, implying that the optical scattering does not significantly affect the cavity finesse.

E. Collisions with Background Gas

We now account for the collisions of the trapped dielectric with the background gas particles. In view of the analysis presented below, we restrict ourselves to a model of damping and decoherence which is valid for semiclassical mechanical states, that is, those whose coherence lengths are smaller than the thermal de Broglie wavelength. A model which is valid for the nanomechanical states in the deep quantum regime can be derived as well but is more complicated and not relevant to this paper [16].

A simplified model representing the effect of the gas background is given by

$$\mathcal{B}[\rho] = -\frac{i\gamma_m}{2\hbar}[\phi, \{L_z, \rho\}] - \frac{I\gamma_m k_B T}{\hbar^2} \mathcal{D}[\phi]\rho, \tag{27}$$

where γ_m is the rate of mechanical damping, T is the ambient temperature, the first term on the right-hand side represents mechanical damping due to gas collisions, and the second term represents the corresponding fluctuations. In writing Eq. (27) a term representing positional diffusion, which is required to ensure the positivity of the density matrix ρ, has been omitted as its effect at the high temperatures considered here is negligible. We note that since we will be concerned below with small amplitudes of torsional motion, the usual problems associated with ϕ not being an explicitly periodic variable do not arise [17].

F. Full Master Equation

Combining the elements from the sections presented above, the full master equation for the probe and nanoparticle angular motion is given by

$$\dot{\rho} = \frac{1}{i\hbar}[H, \rho] + \mathcal{L}_{sc}[\rho] + \mathcal{B}[\rho], \tag{28}$$

where

$$H = H_{OM} + H^{f}_{\text{field}}. \tag{29}$$

G. Classical Langevin Equations

Since our intention is to investigate the system in the classical limit, using standard methods [18], we derive a set of classical Langevin equations from Eq. (28). The first equation determines the time evolution of the (now classical) variable U_l:

$$\dot{U}_l = \frac{i2lU_lL_z}{I}. \tag{30}$$

The second equation describes the change in the angular momentum of the nanoparticle about the beam axis,

$$\dot{L}_z = -\gamma_m L_z - 2il\hbar g_l(U_l - U_l^*)|a(t)|^2 + \tau + \tau_{\text{in}}, \tag{31}$$

where the complex-valued classical variable $a(t)$ is defined such that $|a(t)|^2$ is the number of probe photons inside the cavity at time t, and

$$\tau = \frac{\gamma_{sc}}{2} l_t \hbar \tag{32}$$

is the torque induced by scattering of the trap photons by the nanoparticle. We assume the dielectric is not birefringent, and thus rotational effects due to trap beam polarization are absent. The last term in Eq. (31) is a Langevin torque with zero average obeying the two-time correlation,

$$\langle \tau_{\text{in}}(t)\tau_{\text{in}}(t')\rangle = 2I\gamma_m k_B T\delta(t - t'). \tag{33}$$

Finally, the third equation prescribes the dynamics of the cavity mode,

$$\dot{a} = \left\{ i[\Delta' - \frac{g_l}{2}(U_l + U_l^*)] - \frac{\gamma}{2} \right\} a + \sqrt{\gamma} a_{\text{in}}, \tag{34}$$

where $\Delta' = \Delta - g_l/2$ and $\Delta = \omega_p - \omega_c$ is the detuning between the pump frequency ω_p and the cavity probe mode frequency ω_c. The last term in Eq. (34) has the mean value

$$\langle a_{\text{in}}\rangle = \sqrt{\frac{P_{\text{in}}}{\hbar\omega_c}}, \tag{35}$$

where P_{in} is the input power, and the two-time correlation function is

$$\langle a_{\text{in}}(t)a_{\text{in}}(t')\rangle = \delta(t - t'). \tag{36}$$

3. STABILITY

Equations (30)–(36) were used earlier to analyze full unhindered rotation of the nanoparticle around the ring trap [10]. In that case the azimuthal lattice served as a weak probe of the mechanical motion. In the present situation we consider the opposite limit where the azimuthal lattice is strong enough to trap the nanoparticle at a specific angular position. As we will see below, for this physical situation to prevail, the scattering torque needs to be weaker than the lattice torque, that is,

$$\tau < 4l\hbar g_l |a_s|^2, \tag{37}$$

where $|a_s|^2$ is the steady state probe photon number in the cavity.

A. Steady State Solutions for Torsional Motion

In the steady state the nanoparticle is localized in one of the wells of the lattice, namely, near some $\phi_n = \frac{n\pi}{l}$, where $n = 0, \ldots 2l - 1$, and the steady state angular momentum

$$L_{z,s} = 0, \tag{38}$$

which solves Eq. (30). The remaining steady-state equations give

$$\sin(2l\phi_s) = -\frac{\tau}{4l\hbar g_l |a_s|^2}, \tag{39}$$

which is a relation valid in the regime indicated by Eq. (37) and also implies

$$\cos(2l\phi_s) = -\left[1 - \left(\frac{\tau}{4l\hbar g_l |a_s|^2}\right)^2\right]^{1/2}, \tag{40}$$

where the minus sign has been chosen to be consistent with the fact that in the absence of torque the equilibrium point is where $\sin 2l\phi_s = 0$, $\cos 2l\phi_s = -1$ (see below). Finally, the steady state cavity field is

$$a_s = \frac{\sqrt{\gamma} a_{\text{in}}}{-i[\Delta' - g_l \cos 2l\phi_s] + \frac{\gamma}{2}}. \tag{41}$$

Below we will use the dimensionless steady state cavity intensity,

$$I_s = |a_s|^2. \tag{42}$$

B. Equation of Stability

Before we consider the full equation of stability, we first consider the case $\tau = 0$, which could be arranged physically by the use of an external torque to cancel the effects of trap photon scattering [10]. In this situation, $\phi_s = \phi_n$, $\sin 2l\phi_s = 0$, $\cos 2l\phi_s = -1$, and

$$I_s = \frac{\gamma^2}{(\Delta' + g_l)^2 + \left(\frac{\gamma}{2}\right)^2} I_I, \tag{43}$$

where the dimensionless input intensity is

$$I_I = \frac{|a_{\text{in}}|^2}{\gamma}. \tag{44}$$

In the absence of net torque on the nanoparticle, therefore, the cavity probe intensity is a single-valued function of the input intensity, and the system is monostable. Physically, this corresponds to a situation in which the particle's equilibrium position corresponds to the minimum of a lattice well.

For $\tau \neq 0$, combining Eqs. (39)–(42), we obtain a nonlinear equation for the steady state cavity probe intensity,

$$C_4 I_s^4 + C_3 I_s^3 + C_2 I_s^2 + C_1 I_s + C_0 = 0, \tag{45}$$

where the coefficients are

$$C_0 = \left(\frac{\tau}{4l\hbar}\right)^4, \tag{46}$$

$$C_1 = 2\gamma^2 I_I \left(\frac{\tau}{4l\hbar}\right)^2, \tag{47}$$

$$C_2 = \gamma^4 I_I^2 + \left(\frac{\tau\Delta'}{2l\hbar}\right)^2 - 2\left(\frac{\tau}{4l\hbar}\right)^2 \left[\Delta'^2 + g_l^2 + \left(\frac{\gamma}{2}\right)^2\right], \tag{48}$$

$$C_3 = -2\gamma^2 I_I \left[\Delta'^2 + g_l^2 + \left(\frac{\gamma}{2}\right)^2\right], \tag{49}$$

$$C_4 = \left(\frac{\gamma}{2}\right)^4 + [\Delta'^2 - g_l^2]^2 + \frac{\gamma^2}{2}[\Delta'^2 + g_l^2]. \tag{50}$$

Before we present quantitative solutions to Eq. (45), we make some qualitative remarks below.

C. Stability Analysis

We note that Eq. (45) is nonlinear in the intracavity probe intensity I_s, which indicates the possibility of multistability, introduced by the presence of the torque τ. The degree of Eq. (45) in the variable I_s is four, in contrast to the usual bistability equation of linear vibrational optomechanics, which is of third order in the cavity intensity [19,20].

However, it can readily be shown that the number of physically acceptable (i.e., positive real-valued) solutions of Eq. (45) for I_s is at most two. This follows from the fact that the coefficients C_0, C_1, and C_4 are always positive (for physical values of the system parameters), C_3 is always negative, while C_2 can be either positive or negative depending on the parameters. But in all cases, the number of sign changes of successive coefficients in the polynomial of Eq. (45) is two. By Descartes's rule of signs, therefore, the number of positive real roots is either two or zero. This is in contrast to the standard optomechanics where the number of steady state cavity intensity values is either one or three [19,20].

The appearance and stability behavior of the roots can be understood by considering the interplay between the torques due to trap scattering and the lattice. For simplicity we will present our description in the regime where the optical damping is high, and the mechanical damping and fluctuations are negligible. With these assumptions the cavity probe mode can be eliminated adiabatically from Eq. (34), yielding

$$a = -\frac{\sqrt{\gamma}a_{\text{in}}}{i[\Delta' - g_l \cos 2l\phi] + \frac{\gamma}{2}}, \tag{51}$$

which can be used in Eq. (31) to provide

$$\dot{L}_z \cong \frac{4l\hbar\gamma|a_{\text{in}}|^2 \sin 2l\phi}{[\Delta' - g_l \cos 2l\phi]^2 + \left(\frac{\gamma}{2}\right)^2} + \tau = \tau_{\text{net}}. \tag{52}$$

The first term on the right-hand side represents the torque due to the lattice and the second term the scattering torque. These terms can be integrated to analytically yield the angular potential energy,

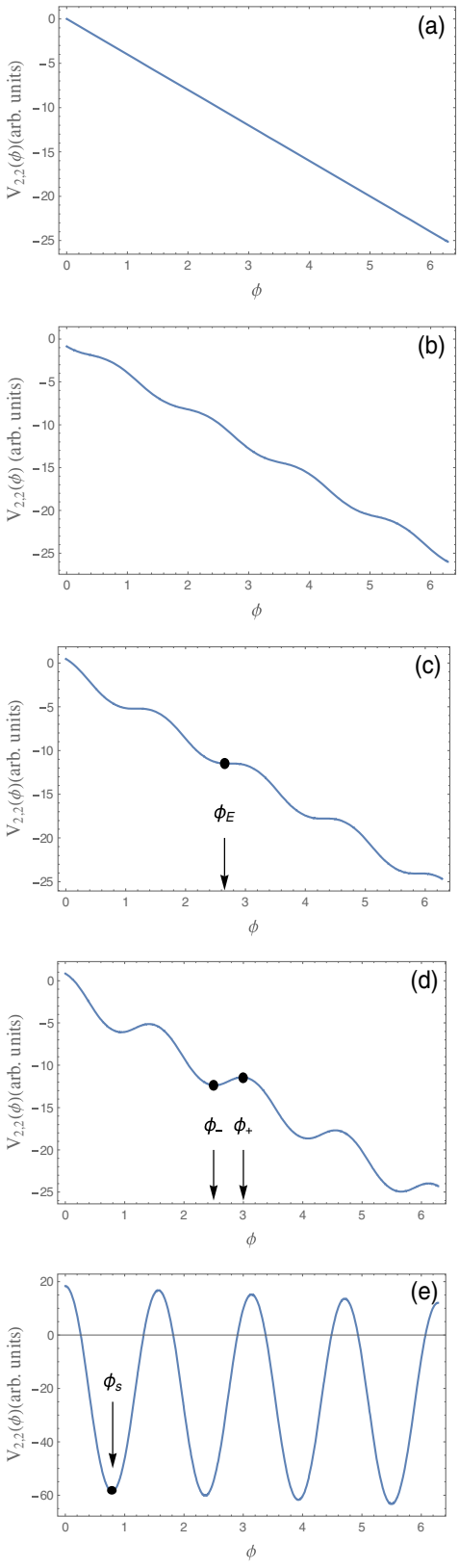

Fig. 2. Angular potential $V_{2,2}(\phi)$ [Eq. (54)] experienced by the nanoparticle for various probe powers increasing from zero, (a) to (e). To ensure visual clarity, parameters used were as follows: $\tau = 2$ Nm, $\Delta' = 0$, $g_l = -1$ Hz, $\gamma = 1$ Hz, $l = l_t = 2$. ϕ_E and ϕ_+ are points of unstable equilibrium, and ϕ_- and ϕ_s are points of stable equilibrium.

$$V_{l,l_t}(\phi) = -\int_0^{\phi}\left\{\frac{4l\hbar\gamma|a_{\rm in}|^2\sin 2l\phi}{[\Delta' - g_l\cos 2l\phi]^2 + \left(\frac{\gamma}{2}\right)^2} + \tau\right\}d\phi \quad (53)$$

$$= -\tau\phi - 4\hbar|a_{\rm in}|^2\left\{\tan^{-1}\left[\frac{2(g_l\cos 2l\phi - \Delta')}{\gamma}\right] - \tan^{-1}\left[\frac{2(g_l - \Delta')}{\gamma}\right]\right\}. \quad (54)$$

Figure 2 shows $V_{2,2}(\phi)$ for various values of probe power. In Fig. 2(a), the probe power is zero; the particle sees only the scattering torque and executes full rotations about the cavity axis. In Fig. 2(b), some probe photons are present in the cavity, but they cannot stop the full rotation, only modulate it at the lattice frequency [10]. In Fig. 2(c), the probe intensity is at a critical value where the net torque vanishes at points such as ϕ_E. Clearly, such points of equilibrium are unstable. In Fig. 2(d), the probe intensity is above threshold and pairs of equilibrium points, $\phi_\pm$, appear. As can be seen, ϕ_- is stable and ϕ_+ is unstable. In Fig. 2(e), the probe intensity is so high that the lattice torque dominates the scattering torque. In this case it can be seen that the minima of the potential occur at $\cos(4\phi_s) = -1$, that is, at $\phi_s = \frac{\pi}{4}, \frac{3\pi}{4}, \frac{5\pi}{4}$, and $7\pi/4$.

A more rigorous analysis, using the Jacobian of the system to determine dynamical stability and without using the mentioned restrictions on optical and mechanical dissipation and noise, yields essentially the same results and will not be presented here.

Using realistic parameters and without using the adiabatic approximation, we show the plot of I_s as a function of I_I—obtained by solving Eq. (45)—in Fig. 3. As can be seen, up until a critical input intensity, there are no equilibria. At this intensity, the (degenerate) solution corresponding to ϕ_E appears. Beyond this critical intensity, two distinct solutions corresponding to $\phi_\pm$ emerge. The upper (stable) branch corresponds to ϕ_- in Fig. 2 since for a given torque (or equivalently I_I), according to Eq. (39), the larger value of I_s occurs for the equilibrium point with smaller ϕ_s. The lower (unstable) branch corresponds to ϕ_+. In units relevant to the experiment, I_I at threshold and for a wavelength of 1064 nm corresponds to about 1 mW of input power into the cavity.

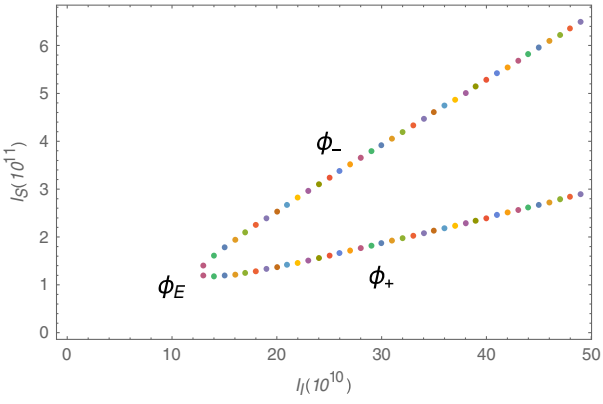

Fig. 3. Stable (ϕ_-) and unstable (ϕ_+) solutions to the intracavity intensity as a function of input intensity, obtained from Eq. (45). Parameters used were $\tau = 10fN$ mm, $m = 1.5\times10^{-19}$ kg, $R = 2$ mm, $r = 150$ nm, $\gamma_m = 60$ Hz, $\Delta' = 0$, $\gamma = 150$ KHz, $g_l = -25$ mHz, $l = l_t = 2$.

4. DYNAMICS ABOUT THE STABLE POINT

In this section we examine the full numerical dynamics of the nanoparticle about the stable equilibrium point ϕ_- [see Fig. 5(d)], which are shown in Figs. 4–6.

In Fig. 4 we consider the situation $\tau = 0$. Figure 4(a) shows the time behavior of the probe photon number as it achieves a

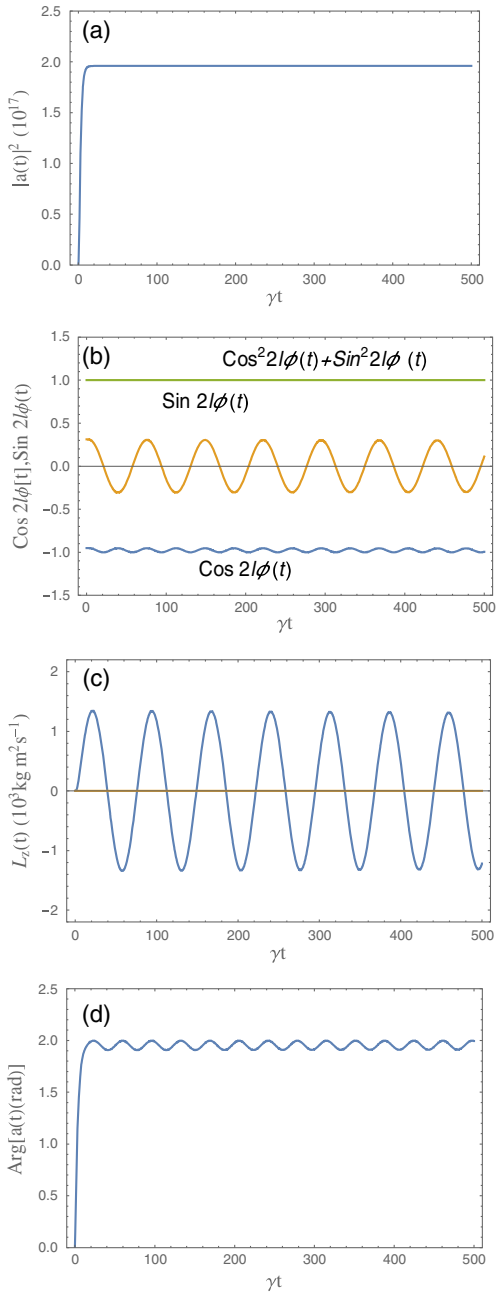

Fig. 4. Full numerical dynamics of the optomechanical system: (a) $|a(t)|^2$, (b) $\cos 2l\phi(t)$ and $\sin 2l\phi(t)$, (c) $L_z(t)$, (d) $\mathrm{Arg}[a(t)]$. All panels were generated using $\tau = 0$, $l = 2$. Other parameters used were the same as in Fig. 3. Initial conditions were set as $a(0) = 0$, $L_z(0) = 0$, $\cos(4\phi)(0) = -0.98$, $g_l = -1$ Hz, $a_{\rm in} \cong 10^{11}$ $\mathrm{s}^{-1/2}$.

steady state in the cavity. It can be seen that any sinusoidal modulation of $|a(t)|^2$ is negligible. In Fig. 4(b), the two quadratures of harmonic motion are shown as functions of time. The oscillation frequency of the sin $4\phi(t)$ curve is 8.6 KHz. That this is the mechanical frequency can be seen by noticing that the amplitude of the sine curve is much smaller than one. Therefore we can linearize sin $4\phi \cong 4\phi$ in Eq. (31) and, ignoring damping, extract the harmonic frequency of oscillation $\omega_m = (32\hbar g_l |a(t \gg \gamma^{-1})|^2 / I)^{1/2}$, which yields 8.7 KHz, quite close to that observed numerically. The cosine curve oscillates at $2\omega_m$, which is to be expected, since to the lowest nontrivial order it is quadratic in the angular displacement. Figure 4(c) shows the harmonic variation of the angular momentum. Since from Eq. (31) we see that L_z is driven by the sine term, it oscillates at ω_m. Figure 4(d) shows that the phase of the cavity field oscillates at $2\omega_m$. This is also reasonable, as Eq. (34) implies the phase of the probe field is driven by the cosine quadrature. It follows that, in contrast to the standard optomechanical setup, the position noise spectrum of the mechanical oscillator can be found by homodyning the cavity output at *twice* the mechanical frequency [21].

In Fig. 5 we consider the case $\tau = 2fN$ mm rad. The dynamics of the probe cavity intensity, as shown in Fig. 5(a), is the same as in Fig. 4(a), as the probe power is the same in both cases. In Fig. 5(b) the sine trace is displaced slightly lower vertically as compared to Fig. 4(b). This reflects the shift in the

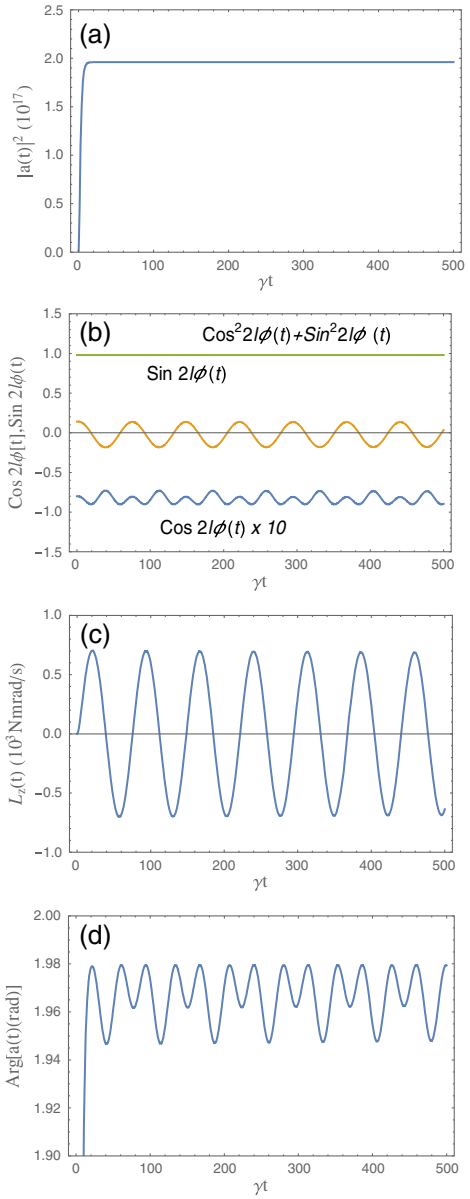

Fig. 5. (a) $|a(t)|^2$, (b) cos $2l\phi(t)$ and sin $2l\phi(t)$, (c) $L_z(t)$, (d) Arg$[a(t)]$. All panels were generated using $\tau = 2fN$ mm. Other parameters used were the same as in Fig. 4.

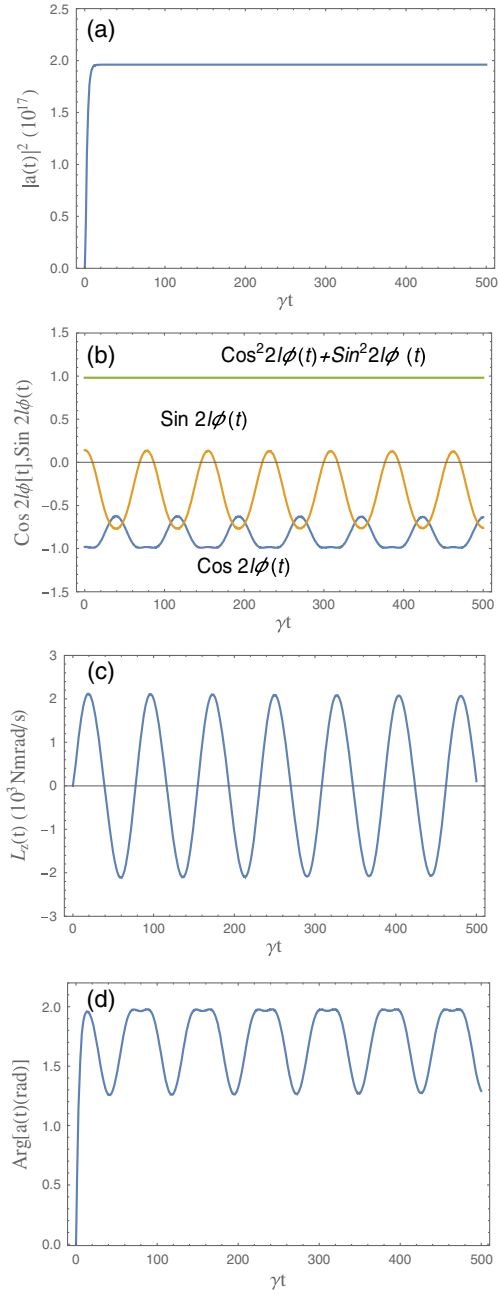

Fig. 6. (a) $|a(t)|^2$, (b) cos $2l\phi(t)$ and sin $2l\phi(t)$, (c) $L_z(t)$, (d) Arg$[a(t)]$. All panels were generated using $\tau = 30fN$ mm. Other parameters used were the same as in Fig. 4.

nanoparticle equilibrium position caused by the torque τ; see Eq. (39). The cosine trace, which has been scaled up by a factor of 10 for visibility, now shows both frequencies ω_m as well as $2\omega_m$. This is because the presence of the torque now causes a term linear in ϕ to appear in the expansion of cos 4ϕ in addition to the term quadratic in ϕ for small angular displacements. Physically, this corresponds to the introduction of linear optomechanical coupling in Fig. 5 as compared to Fig. 4, where only quadratic coupling exists. In Fig. 5(c) the angular momentum oscillates at ω_m. In Fig. 5(d) the time evolution of the phase of the cavity probe field shows both ω_m and $2\omega_m$ dependence.

In Fig. 6 we consider a larger torque $\tau = 30fN$ mm rad, which causes a substantial linear optomechanical coupling. The probe intensity is shown in Fig. 6(a). In Fig. 6(b), the sine curve is shifted even further down compared to Fig. 5(b). The cosine curve has a small component at $2\omega_m$, but the major frequency present is ω_m. In Fig. 6(c), the angular momentum oscillates at ω_m. In Fig. 6(d), the cavity probe phase shows oscillations mostly at ω_m.

From the above analysis we conclude that the relative strength of linear versus quadratic couplings can be detected experimentally in the proposed system by homodyning the output of the cavity.

5. CONCLUSIONS

In this paper we have explored the off-axis torsional optomechanics of a levitated nanoparticle confined in a cavity driven by optical beams carrying OAM. We have shown that scattering torque from the trapping beam creates an instability in the system. We have also demonstrated that the dynamics around the stable equilibrium allow the use of the optical torque for tuning the linear optomechanical coupling in this system, and also a way to detect the relative strengths of the two couplings by homodyning the probe field exiting the cavity. To support our calculations, we have derived a quantum master equation for the system and used it to derive classical Langevin equations on which our analysis is based. Our investigations are likely to be of interest to researchers exploring quantum mechanics using torsional optomechanics, and could be extended to atomic systems such as have been recently proposed for realizing time crystals [22].

Funding. National Science Foundation (NSF); Directorate for Mathematical and Physical Sciences (MPS) (1454931); Office of Naval Research (ONR) (N00014-14-1-0803); Research Corporation for Scientific Advancement (RCSA) (20966).

Acknowledgment. We thank Wenchao Ge for useful discussions.

REFERENCES

1. J. Gieseler, B. Deutsch, R. Quidant, and L. Novotny, "Subkelvin parametric feedback cooling of a laser-trapped nanoparticle," Phys. Rev. Lett. **109**, 103603 (2012).
2. L. P. Neukirch, E. von Haartman, J. M. Rosenholm, and A. N. Vamivakas, "Multi-dimensional single-spin nano-optomechanics with a levitated nanodiamond," Nat. Photonics **9**, 653–657 (2015).
3. J. Millen, T. Deesuwan, P. Barker, and J. Anders, "Nanoscale temperature measurements using non-equilibrium Brownian dynamics of a levitated nanosphere," Nat. Nanotechnol. **9**, 425–429 (2014).
4. O. Romero-Isart, A. C. Pflanzer, F. Blaser, R. Kaltenbaek, N. Kiesel, M. Aspelmeyer, and J. I. Cirac, "Large quantum superpositions and interference of massive nanometer-sized objects," Phys. Rev. Lett. **107**, 020405 (2011).
5. N. Kiesel, F. Blaser, U. Delic, D. Grass, R. Kaltenbaek, and M. Aspelmeyer, "Cavity cooling of an optically levitated submicron particle," Proc. Natl. Acad. Sci. USA **110**, 14180–14185 (2013).
6. J. Gieseler, M. Spasenovic, L. Novotny, and R. Quidant, "Nonlinear mode coupling and synchronization of a vacuum-trapped nanoparticle," Phys. Rev. Lett. **112**, 103603 (2014).
7. O. Romero-Isart, M. L. Juan, R. Quidant, and J. I. Cirac, "Toward quantum superposition of living organisms," New J. Phys. **12**, 033015 (2010).
8. H. Shi and M. Bhattacharya, "Coupling a small torsional oscillator to large optical angular momentum," J. Mod. Opt. **60**, 382–386 (2013).
9. T. M. Hoang, Y. Ma, J. Ahn, J. Bang, F. Robicheaux, Z.-Q. Yin, and T. Li, "Torsional optomechanics of a levitated nonspherical nanoparticle," Phys. Rev. Lett. **117**, 123604 (2016).
10. M. Bhattacharya, "Rotational cavity optomechanics," J. Opt. Soc. Am. B **32**, B55–B60 (2015).
11. M. Mazilu, Y. Arita, T. Vettenburg, J. M. Auñón, E. M. Wright, and K. Dholakia, "Orbital-angular-momentum transfer to optically levitated microparticles in vacuum," Phys. Rev. A **94**, 053821 (2016).
12. O. Romero-Isart, A. C. Pflanzer, M. L. Juan, R. Quidant, N. Kiesel, M. Aspelmeyer, and J. I. Cirac, "Optically levitating dielectrics in the quantum regime: theory and protocols," Phys. Rev. A **83**, 013803 (2011).
13. C. C. Gerry and P. L. Knight, *Introductory Quantum Optics* (Cambridge University, 2004), p. 23.
14. K. Kowalski, J. Rembielinski, and L. C. Papaloucas, "Coherent states for a quantum particle on a circle," J. Phys. A **29**, 4149–4167 (1996).
15. C. W. Gardiner and P. Zoller, in *Quantum Noise: A Handbook of Markovian and Non-Markovian Quantum Stochastic Methods with Applications to Quantum Optics* (Springer, 2004).
16. B. A. Stickler, S. Nimmrichter, L. Martinetz, S. Kuhn, M. Arndt, and K. Hornberger, "Rotranslational cavity cooling of dielectric rods and disks," Phys. Rev. A **94**, 033818 (2016).
17. P. Carruthers and M. M. Nieto, "Phase and angle variables in quantum mechanics," Rev. Mod. Phys. **40**, 411–440 (1968).
18. M. O. Scully and M. S. Zubairy, *Quantum Optics* (Cambridge University, 2012).
19. C. Genes, D. Vitali, P. Tombesi, S. Gigan, and M. Aspelmeyer, "Ground-state cooling of a micromechanical oscillator: comparing cold damping and cavity-assisted cooling schemes," Phys. Rev. A **77**, 033804 (2008).
20. R. Ghobadi, A. R. Bahrampour, and C. Simon, "Quantum optomechanics in the bistable regime," Phys. Rev. A **84**, 033846 (2011).
21. M. Aspelmeyer, T. J. Kippenberg, and F. Marquardt, "Cavity optomechanics," Rev. Mod. Phys. **86**, 1391–1452 (2014).
22. H.-K. Li, E. Urban, C. Noel, A. Chuang, Y. Xia, A. Ransford, B. Hemmerling, Y. Wang, T. Li, H. Häffner, and X. Zhang, "Realization of translational symmetry in trapped cold ion rings," Phys. Rev. Lett. **118**, 053001 (2017).